Ab Initio Excited State Properties and Dynamics of a Prototype σ-Bridged-Donor−Acceptor Molecule

Enrico Tapavicza,[†] Ivano Tavernelli, and Ursula Rothlisberger*

Laboratory of Computational Chemistry and Biochemistry, Ecole Polytechnique Fédérale de Lausanne, Lausanne, Switzerland

Received: February 13, 2009; Revised Manuscript Received: May 23, 2009

The photophysical and dynamical properties of the donor−(σ-bridge)−acceptor molecule *N*-phenylpiperindone-malondinitrile are investigated by second-order approximate coupled cluster (CC2) and time-dependent density functional theory (TDDFT). The study is based on optimized equilibrium geometries for ground and excited states as well as on ab initio molecular dynamics simulations. While CC2 and DFT both predict ground state geometries that are consistent with the crystal structure, equilibrium geometries for the fluorescent charge transfer (CT) state are qualitatively different between CC2 and TDDFT. CC2 reproduces the experimental results for vertical excitations (within 0.3 eV) and provides an orbital assignment of the experimental absorption bands that is supported by experiments. Using CC2, a good agreement is also found for fluorescence energies (within 0.1−0.6 eV). At contrast, CT absorption and fluorescence energies are strongly underestimated by TDDFT using the semi-local functional PBE but improved agreement is found for the hybrid functional PBE0. However, for both functionals, TDDFT fails to predict an equilibrium geometry of the intradonor excited state because of mixing between this state and an artificially low-lying CT state during the optimization. This is an example where the well documented CT failure of TDDFT affects properties of other locally excited states. The minimum of the intradonor locally excited state was therefore only located by the CC2 method. The internal conversion (IC) process from a locally excited donor state to the CT state is simulated by excited state ab initio molecular dynamics based on CC2 and where nonadiabatic transitions are described using the Landau−Zener approximation. We find the IC process to occur a few tens of femtoseconds after excitation. The simulation provides a detailed description of the atomic rearrangements in electron donor and acceptor that drive the interconversion process.

1. Introduction

Organic donor−bridge−acceptor (DBA) systems have a long history as model systems for the basic understanding of elementary processes of photoinduced electron transfer (ET) in photosynthesis.[1] Furthermore, these types of systems are becoming attractive as possible building blocks in nano-optics and molecular electronics.[2−4]

DBA molecules with saturated hydrocarbon bridges (D-σ-A) were first studied in the context of through-bond interactions[5,6] (TBI), which refers to the interaction of electron donor and acceptor orbitals through mutual mixing with saturated σ-bond orbitals that separate the two functional groups. It has been hypothesized and shown experimentally that TBI leads to structural distortions of DBA molecules compared to the molecular structures of the single donor, acceptor, and bridge units.[7−12] In addition, TBI leads to strong charge transfer (CT) absorption bands and excited states with large dipole moments[13] that often show strong fluorescence and phosphorescence.[14,15]

The physical properties of D-σ-A molecules make them especially suited to build molecular rectifiers[16−18] and because of their large hyperpolarizability, they are also suited for frequency doubling of laser light.[19−21] In addition, these compounds can undergo remarkable structural changes caused by intramolecular electron transfer (ET), which can occur upon photoexcitation. This phenomena, also known as Coulomb induced folding or harpooning,[22,23] is of potential interest for applications in photoswitches.[24]

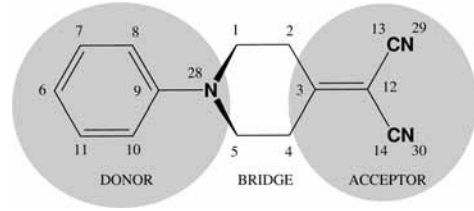

Figure 1. *N*-Phenylpiperidone-malondinitrile, which serves as the DBA model in the present study. The definition of donor (D), bridge (B), and acceptor (A) used in the analysis as well as the atomic numbering are indicated.

In general, intramolecular ET is thought to proceed by two phenomenologically different pathways, namely optical ET and photoinduced ET.[25] In optical ET the transfer of an electron proceeds directly by excitation while in photoinduced ET an excitation occurs first into a locally excited (LE) state that then couples via molecular rearrangements to the CT state.

The class of D-σ-A molecules containing piperidine and hexylidene as central bridging units[12,13,19,26−29] have been recently rediscovered as building blocks for materials.[30−32]

In this study we focus on the simplest member of the class of piperidine-bridged compounds, N-phenylpiperidone-malondinitrile (DA1), depicted in Figure 1. In DA1, an N-phenyl unit serves as the electron donor and is separated from the dicya-

* To whom correspondence should be addressed. E-mail: ursula.roethlisberger@epfl.ch.

[†] Present address: University of California, Irvine, Department of Chemistry, 1208 Natural Sciences II, Irvine CA 92697-2025.

10.1021/jp901356k CCC: $40.75
Published on Web 08/07/2009

noethylene electron accepting moiety by three saturated σ-bonds of the central piperidine unit. DA1 is characterized by a strong CT absorption and a high fluorescence quantum yield. It has been found that excitation at different wavelengths all lead to a single fluorescence band, which is caused by emission from the lowest CT state.[13] This indicates the coexistence of both optical and photoinduced ET.

The aim of our study is to investigate the optical properties of DA1, explain the high fluorescence quantum yield, and gain information of the structural rearrangements associated with the ET. Furthermore, the mechanism of internal conversion (IC) from a LE donor state to the CT state is investigated.

Very recently, first principles excited-state electronic-structure methods have been used to complement experimental studies of donor−acceptor systems, in particular for the rational design of molecules with tailored electronic and optical properties.[33−42] Within this context, our aim is also to probe the quality and performance of different excited-state methodologies for the description of this class of systems.

Coupled cluster (CC) methods[43] provide size-extensive descriptions of excited state properties of molecular systems at a lower cost than configuration interaction methods. Among CC methods, second-order approximate CC singles-and-doubles[44] (CC2) offers a good comprise between accuracy and computational efficiency. CC2 is an approximation to coupled cluster singles and doubles (CCSD) but exhibits an N^5 scaling with the number of orbitals rather than the N^6 scaling of CCSD. In addition, excitation energies can be obtained by a linear response (LR) treatment of the CC2 reference state. CC2 excitation energies have been shown to be within 0.3 eV from experimental measurements for a variety of systems.[45,46] Since in LR-CC2, double excitations are only treated approximately, excitation energies can be expected to be accurate only if single excitations are the dominant contribution. Reasonable accuracy was found if the double excitation amplitudes did not exceed 10%.[47,48] In addition, being a single reference method, CC2 is expected to fail to describe intersections between excited states and the reference state. However, in highly fluorescent molecules as the present one, conical intersections between ground and excited states only play a minor role. Within these limits, CC2 has been successfully applied to study photophysical processes in a range of different systems.[49−59]

Further reduction of computational cost can be obtained by using time-dependent density functional theory (TDDFT).[60−62] This method has been successfully applied to study the photochemistry and photophysics of different systems.[63−72] Unfortunately, TDDFT has some severe drawbacks related to the approximate nature of the exchange-correlation (xc) kernel, which still restricts its general usage for a large variety of systems.[73] One of the major problems of TDDFT for extended systems is related to the well-known underestimation of long-range CT excitations[74] that has also been found to modify potential energy surfaces leading to erroneous excited state geometries.[75] However, in some cases sufficient overlap between donor and acceptor orbitals can lead to a reasonable description of CT states,[66,76−78] especially when hybrid functionals are used. In the light of all this, we also explore the quality of TDDFT for the CT states occurring in DA1, in addition we probe to what extent a possible CT failure can affect the description of LE states.

2. Computational Details

All calculations presented here were performed with the TURBOMOLE[79] program package. Geometry optimizations in the ground state were carried out using CC2 and DFT. The excited state geometries were obtained from LR-CC2 and LR-TDDFT. All geometry optimizations employed the TZVP[80] basis set with default convergence criteria for Cartesian gradients (10^{-3} a.u.) and total energies (10^{-6} a.u.). Improved excitation energies and excited state properties were obtained by single-point calculations using the augmented aug-cc-pVDZ[81] basis set for both, CC2 and TDDFT. Excitation energies were computed at LR-CC2[44] level and by LR-TDDFT[61] within the Tamm-Dancoff approximation (TDA).[82] In the notation used in the following CC2 stands for both, ground state CC2 and LR-CC2. Furthermore, the abbreviation TDDFT stands for LR-TDDFT within the TDA.

The CC2 module of TURBOMOLE[45,46,83,84] makes use of the frozen core approximation. In our calculations the 17 lowest molecular orbitals were kept frozen. In addition, the Coulomb repulsion is approximated by the resolution of identity (RI) method.[85] Therefore optimized auxiliary basis sets for SVP, TZVP,[80] and aug-cc-pVDZ[86] basis sets were used.

The DFT and TDDFT implementations of TURBOMOLE are described in refs 87−90. Calculations employ the PBE[91] xc-functional and its hybrid version PBE0, in which 25% of PBE exchange is replaced by exact (Hartree−Fock) exchange. Corresponding TDDFT calculations are denoted by TDPBE and TDPBE0 in the following.

Ground state Born−Oppenheimer AIMD in the NVT ensemble was performed on the PBE/SVP level of theory. A Nosé-Hoover thermostat with a target temperature of 300 K and a characteristic response time of 100 au was applied to maintain a constant temperature. A time step of 30 au ($\approx$0.73 fs) was used and the simulation was carried out for a total of 1.5 ps.

Excited state AIMD was performed using ground and excited state energies and nuclear forces computed on CC2/SVP level. The smaller basis set leads to an upshift of all relevant excitation energies of about 0.1 eV. Therefore, our primary interest, the energy gap between LE and CT state is not affected by the smaller basis set. In contrast to the ground state simulation, excited state AIMD was done in the NVE ensemble and a time step of 15 au ($\approx$0.36 fs) was used. A total of 8 excited state simulations of 20−150 fs were done.

3. Results

3.1. Ground State Geometries. The ground state equilibrium structure of DA1 was optimized with CC2, DFT/PBE, and DFT/PBE0. Selected bond distances, angles, dihedral angles and the complete Cartesian coordinates are reported in Tables 1, 4 and 5 of the Supporting Information.

While for the D, B, A units themselves only small deviations from the crystal structure are found, the theoretical structures and the crystal structure differ in the twist angle around the N28−C9 bond, defining the orientation of the phenyl ring relative to the piperidine moiety. The comparison of the Newman projections along the N28−C9 bond (Figure 2) shows that all theoretical methods predict a rather asymmetric conformation, in contrast to the crystal structure that nearly conserves a symmetry plane perpendicular to the plane of the phenyl ring.

Regarding the pyramidalization angle at N28 (Table 1), DFT structures and the crystal structure exhibit a flatter conformation than the CC2 structure.

The same trend is found for the acceptor, where CC2 again predicts a slightly stronger pyramidalization of the C3 center (Table 2) than DFT and experiment.

Theoretical structures agree within a root mean square deviation (RMSD) of the nuclear coordinates of 0.18 Å with

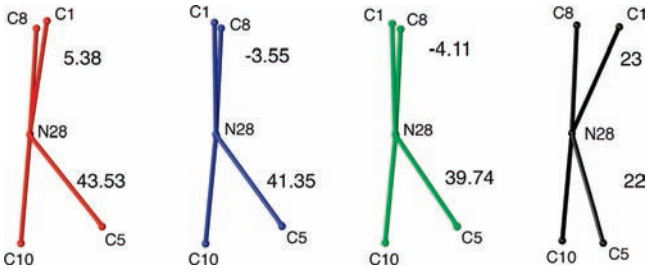

Figure 2. Newman projection along the N28−C9 bond. Red, CC2; blue, PBE; green, PBE0; and black, crystal structure.

TABLE 1: *N*-Pyramidalization Angles (°) of Ground (S_0) and the First Two Excited States (S_1 and S_2) Geometries Calculated with CC2, (TD)DFT, and Obtained from X-ray Diffraction Data[12a]

	DA1				NPP		
	CC2	PBE	PBE0	X-ray	CC2	PBE	PBE0
S_0	26.38	19.25	17.83	21.62	26.02	14.74	17.25
S_1	12.60(10.21)	−7.70	−4.84				
S_2	15.04						

[a] The average of the dihedrals C1−C5−C9−N28, C5−C9−C1−N28, and C9−C1−C5−N28 define the *N*-pyramidalization angle. Atom numbers are defined in Figure 1. For CC2, the value of Conformer II (defined in Figure 4) is given in parentheses.

TABLE 2: Calculated and Experimental[12] Values of the C3-Pyramidalization Angle (°) of Ground (S_0) and First Two Excited States (S_1 and S_2) Geometries of DA1[a]

	CC2	PBE	PBE0	X-ray
S_0	4.87	4.30	2.49	2.66
S_1	29.19(−22.70)	−26.68	−21.34	
S_2	3.14			

[a] The C3-pyramidalization angle is defined as the average of the dihedrals C2−C12−C4−C3, C12−C4−C2−C3, and C4−C2−C12−C3. For CC2, the value of Conformer II (defined in Figure 4) is given in parentheses.

one another. They differ by about 0.24−0.29 Å from the crystal structure. In contrast, if we consider the donor, bridge, and acceptor units on their own then a deviation of <0.07 Å with the experiment is found. The fact that all theoretical gas-phase structures predict this asymmetric conformation suggests that the more symmetric conformation of the crystal structure might arise from packing effects.

Different geometric parameters have been found to be sensitive for TBI. In the case of two or more π-systems interacting through three σ-bonds, an elongation of the central bond has been found in various cases.[7−11] As possible reason for this elongation Dougherty et al. proposed a weakening of the central σ-bond due to mixing of the central σ-orbital with π*-orbitals of the chromophore and mixing of the central σ*-orbital with the π-orbital of the chromophore.[7,8]

In the case of DA1, the central C−C bonds of the bridge unit (C1−C2, C4−C5) are expected to be elongated if an interaction between the donor and acceptor is present. For DA1 an elongation due to TBI of about 0.02 Å has been estimated by comparison of different crystal structures.[12] To probe the influence of TBI on the geometry of the σ-relay of the bridge unit we optimized the geometry of N-phenyl piperidine (NPP). NPP may be considered as a DA1 molecule lacking the acceptor moiety, so that distortions due to TBI should be absent. All theoretical methods used here predict central C−C bonds that are about 0.02−0.03 longer compared to the corresponding bonds in NPP (Table 4 in SI) and thus seem to confirm the presence of TBI.

In summary, CC2 and DFT ground state structures are very similar apart from deviations in the pyramidalization angles.

3.2. Vertical Absorption Energies. Using CC2, TDPBE, and TDPBE0 in combination with the aug-cc-pVDZ basis set, we computed the lowest vertical singlet excitation energies from the corresponding optimized ground state geometry (Table 3).

The electronic transitions are interpreted in terms of single-particle transitions between the frontier orbitals of the given reference state. In the case of DFT, these are the Kohn−Sham (KS) orbitals (Figure 3, left) and for CC2 these are the HF orbitals (Figure 3, right). Because of the different nature of KS and HF orbitals, TDDFT and CC2 excited states are not fully comparable. However, regarding localization and nodal structure of the orbitals a comparison is still informative for the nature of the excited state.

For the lowest four excited states, CC2/aug-cc-pVDZ predicts t_1 amplitudes larger than 90% and thus the error due to the approximate description of double excitations can be expected to be small.[47,48] Vertical absorption energies agree within 0.3 eV with the position of the maxima of the experimental bands. We assign the first experimental band at 3.63 eV to the lowest charge transfer excitation ($\pi_D-\pi_A^*$, H → L+6) calculated at 3.69 eV, an assignment that is also supported by the fluorescence experiments of Hermant et al.[13] The next band at 4.25 eV is assigned to an intradonor (ID) ($\pi_D-\pi_D^*$, H → L+14) transition at 4.55 eV, typical for aniline derivatives.[92] According to CC2, the band at 4.99 eV belongs to either another CT excitation (H → L) and/or to a Rydberg like transition (H → L+3/L+2). We find that the accurate description of the latter two states requires the inclusion of diffuse basis functions.

Turning to the TDDFT excitation energies, we see that TDPBE drastically underestimates the lowest CT excitation by more than 1.6 eV. In addition, there are two additional CT states between S_1 and the ID excitation at 4.1 eV that are absent in the CC2 description. Usage of the hybrid xc-functional PBE0 leads to a blue shift of all excitation energies. This blue shift is larger for CT excitations, resulting in a smaller error for the lowest excitation energy compared to TDPBE. With TDPBE0 the artificially low CT state (H-1 → L) is shifted 0.1 eV above the ID state but mixes considerably with the ID state at 4.6 eV. This mixing also affects other excited state properties, for instance the dipole moment of S_2 predicted by TDPBE0 (11.7 D) is considerably larger than the one predicted by CC2 (2.3 D). As we will see in section 3.4, the mixing between ID and CT states also affects the nuclear forces and makes it impossible with TDPBE and TDPBE0 to perform MD in the pure ID state and to optimize the equilibrium geometry.

3.3. Geometries of the Excited Charge Transfer State and Fluorescence Energies. In order to investigate structural rearrangements related to the electron transfer from donor to acceptor and to predict the fluorescence spectra, we optimized the geometry of DA1 in the lowest CT state using CC2, TDPBE, and TDPBE0. Cartesian coordinates, bond lengths, and angles of the S_1 optimized structures are summarized in Tables 2, 4 and 5 in the Supporting Information. According to Hermant et al.,[13] it is this CT state from which the experimentally measured fluorescence is emitted. Using CC2, we find two different geometric minima for the CT state. Both structures show a large increase of the C3 pyramidalization on the acceptor compared to the ground state structure, but they differ in the direction of the pyramidalization (Figure 4, Table 2). The first structure

TABLE 3: Lowest Lying Singlet Excitation Energies ω (eV) of DA1 and Excited State Dipole Moments μ (Debye)[a]

CC2				PBE			PBE0			expt.[b]	
ω(f)	assignment	t_1	μ	ω(f)	assignment	μ	ω	assignment	μ	$\omega(\varepsilon)$	μ
3.69 (0.236)	55% H L+6 8% H-3 L+6 8% H L CT	90.7%	19.1	**2.20** (0.150)	H L CT	16.6	**3.20** (0.046)	π_D-π_A^* CT	19.0	**3.63** (0.118)	18.8
4.55 (0.022)	46% H L+14 9% H L+12 7% H L+13 ID	91.6%	2.3	**3.34** (0.009)	H-1 L CT	23.9	**4.61** (0.008)	51% π_D-π_D^* 43% π_D-π_A^* ID/CT	11.7	**4.25** (0.079)	-
4.886 (0.051)	64% H L 5% H-3 L+6 5%H L+6 CT	93.0%	5.6	**3.75** (0.012)	H L+2 CT	23.2	**4.76** (0.010)	56% π_D-π_A^* 37% π_D-π_D^* CT/ID	15.3	**4.99** (1.000)	
5.03 (0.072)	20% L L+3 15% H L+2 11% H L+12 Rydberg	93.1%	5.7	**4.07** (0.022)	H L+1 ID	0.8	**4.98** (0.081)	π_D-π_D^* ID	7.3		
				4.25 (0.012)	56% π_D-π_A^* 33% π_D-π_A^* ID/CT	9.7	**5.22** (0.133)	55% π_D-π_A^* 9% π_D-π_D^* CT/ID	6.6		

[a] Oscillator strengths f (length representation) and normalized extinction coefficients ε for the experiment are given in parentheses. For CC2 also the percent of the single excitation amplitudes (t_1) are given. All values are computed using the aug-cc-pVDZ basis set. Assignments of the TDDFT spectra are interpreted in terms of KS orbitals (Figure 3, left); CC2 transitions are given on the basis of HF orbitals (Figure 3, right). For transitions whose main contribution is below 65% also the second (and third) contributions are given. According to the location of the orbitals the excitations were labeled as charge transfer (CT), intra-donor (ID), or Rydberg excitations. [b] The experimental values measured in *n*-hexane are taken from ref 13.

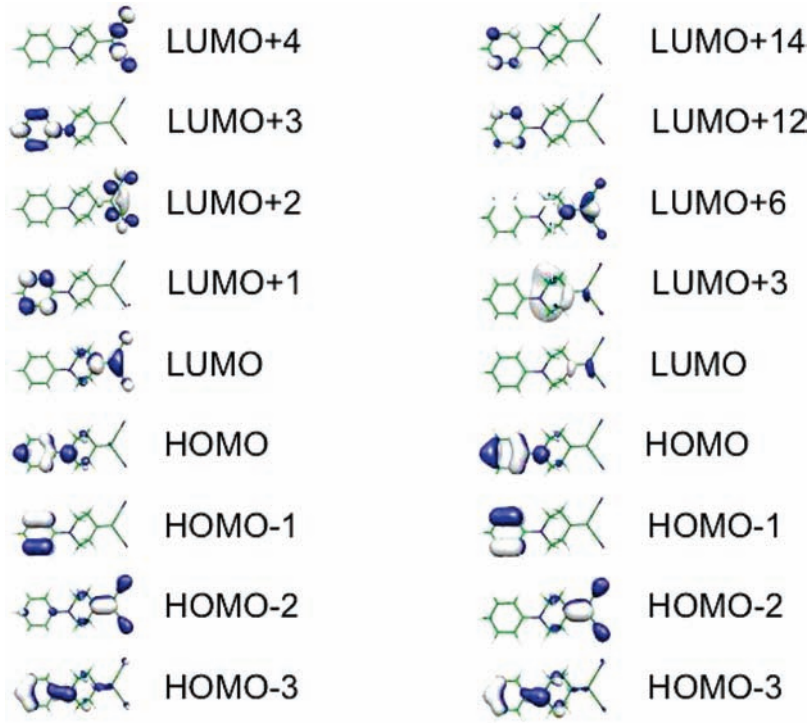

Figure 3. Left: PBE Kohn−Sham molecular orbitals obtained using the aug-cc-pVDZ basis set. Right: Hartree−Fock molecular orbitals obtained using the aug-cc-pVDZ basis set. Assignments of TDDFT transitions are qualitatively given on the basis of the KS orbitals on the left. CC2 transitions are given on the basis of the HF orbitals on the right.

(Conformer I, Figure 4, green) is stabilized by ≈0.1 eV with respect to the other structure (Conformer II, Figure 4, cyan). In addition we observe a flattening of the pyramidalization of the donor nitrogen (Table 1), while the piperidine spacer changes very little. For the bent CT geometry (Conformer II), we observe a change of the sign of the N28−C9 twist angle (Figure 4, left) compared to the ground state geometry (Figure 2, left). Conformer I in contrast exhibits a rather symmetric conformation of the phenyl ring relative to the piperidine moiety (Figure 4, left).

These geometric rearrangements lead to stable CT geometries, but in view of the small rearrangements this can not be considered as harpooning. The pyramidalization of C3 indicates that the negative charge is mainly located on the

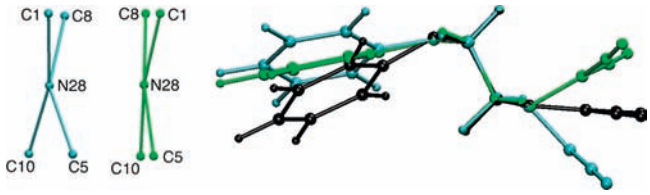

Figure 4. Comparison of the CC2 S_0 geometry (black) and the two different CC2 S_1 geometries. Conformer I (green) is stabilized by ≈0.1 eV with respect to Conformer II (cyan). Left: Newman projection along the N28−C9 bond of the CC2 structures optimized in S_1. Right: CC2 optimized geometries of S_0 and of S_1, aligned on the bridging moiety.

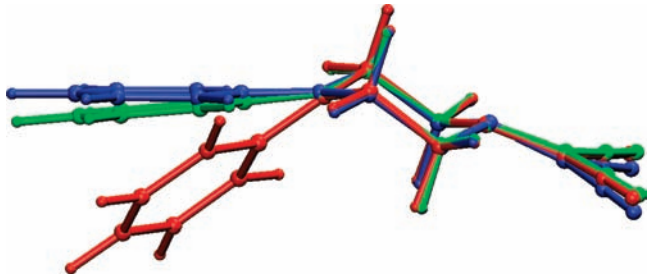

Figure 5. Geometries optimized in the S_1 CT state. Red, CC2; blue, PBE; and green, PBE0. The structures were aligned on the bridging moiety.

C3 atom that connects bridge and acceptor and not on the CN groups of the acceptor. This explains the experimental finding that no folded CT geometries are found if the connecting atom can stabilize a negative charge.[93,94]

Similar to CC2, TDDFT predicts an increase of the N28−C9 twist angle and a similar C3-pyramidalization of the ethylene moiety. In the case of TDDFT, only one direction of the pyramidalization is found. However, regarding the entire molecule, TDDFT structures are qualitatively different from the corresponding CC2 structures (Figure 5) as they do not exhibit the same bending of the molecule at N28. TDDFT assumes structures that are even more linear, due to a flat and slightly inverted conformation of the N28 pyramidalization (Table 1).

To gain insight into the nature of DBA fluorescence, we computed the excitation energies using the aug-cc-pVDZ basis set (Table 4) for the geometries relaxed in the CT state. CC2 predicts a gas phase fluorescence energy of about 1.9 and 2.1 eV, very similar to the experimental value of 2.2 eV in polar solvent. Interestingly the CC2 gas phase value is considerably lower than the experimental value measured in apolar solvent (2.7 eV). However, on the basis of the present calculations, it is not clear whether this difference arises because of a destabilization by the solvent or whether it is due to approximations in the CC2 model.

Similar to the case of the vertical excitation spectra, TDPBE and TDPBE0 drastically underestimate the S_1-S_0 gap, predicting fluorescence energies of 0.34 and 1.63 eV, respectively.

3.4. Geometries of the Intradonor Excited State. Hermant and co-workers[13] found that irrespective of the excitation wavelength a fluorescence typical for the CT state is always observed, leading to the conclusion that the LE states might interact with the CT states. To gain information about the interconversion process, we optimized the geometry of DA1 in the $\pi_D-\pi_D^*$ ID state using the CC2/TZVP method. The corresponding optimization using TDDFT is not possible because the ID state mixes with one of the artificially low-lying CT states and transforms adiabatically into the CT state. The mixing of the adiabatic states is caused by degenerate Kohn−Sham states. In the case of TDPBE0, LUMO+2 and LUMO+1 (Figure 3) cross during the optimization and the initial character of the LE state ($\pi_D-\pi_D^*$) changes into a CT state when LUMO+1 adopts the character of the π_A^* orbital. For this reason no local minimum for the ID state can be located using either TDPBE or TDPBE0, showing that the presence of artificially low-lying CT states in TDDFT can effect properties of non-CT states. Therefore we report only the result of the CC2 optimization (Figure 6, Cartesian coordinates, bond lengths, and angles are given in Tables 3, 4 and 5 in the Supporting Information).

According to the CC2 result, the structural changes in the ID state are much smaller than in the CT state (Figure 6). The most significant change observed is the inversion of the sign of the N28−C9 twist angle (Figure 6, left) similar to the S_1 geometry. Twisting around the N−C bond in the LE state is typical for dialkylanilino derivatives.[66] In dimethylaniline compounds, twisting proceeds until an orthogonal conformation between the phenyl ring and the plane formed by the methyl groups and the nitrogen atom is reached. In the case of DA1, the twist angle does not exceed 90°, which is most likely due to steric hindrance due to the piperidine moiety. In addition the ID optimal structure is characterized by a distortion of the planarity of the phenyl ring (Table 5).

Regarding the CC2 excitation energies at the ID minimum energy structure (Table 6), we observe a decrease of the gap between S_1 and S_2 during the optimization from initially 0.9 to 0.55 eV. We conclude that although the gap between the CT state and the ID state decreases, there is still thermal activation needed to decrease the gap further and allow IC from the ID to the fluorescent CT state. To investigate the process of IC from the ID to the CT state in more detail, we have carried out on the fly excited state CC2 ab initio molecular dynamics (AIMD) simulations described in the next section.

4. Molecular Dynamics

Ground state AIMD at 300 K confirms the hypothesis of a dynamical equilibrium between a conformer with the phenyl group in axial position and one with the phenyl group in equatorial position. This equilibrium was suggested on the basis of experiments and the theoretical argument that CT absorption is thought to be more pronounced for the axial conformer.[12]

From the ground state trajectory, we have chosen 8 different initial geometries for excited state MD. These geometries were vertically excited into the ID (S_2) state, random velocities of a Boltzmann ensemble of 300 K were generated, and the nuclear positions were propagated in time along the CC2 excited state forces. During the simulation, the energy gap between ID and CT state is monitored. In case of an avoided crossing (AC), i.e. a minimum of the S_1-S_2 gap, the Landau−Zener probability P_{LZ} is evaluated.[95] Within the first 22 fs, all simulations exhibit a minimum of the S_1-S_2 energy gap of 0.07−0.27 eV, leading to transition probabilities between 45−96% (Table 7). At later times we find additional ACs with transition probabilities up to 99%. This suggests a fast IC process, confirming the assignment of the broad second absorption band[13] to the ID excitation.

From the first 20 fs of the representative trajectory shown in Figure 7 we see that the AC is separated from the Franck−Condon region by an energetic barrier and lies higher in energy than the Franck−Condon region. In all simulations activation energies E_A of 0.3−1.3 eV are needed in order to reach the AC (Table 7). If the system is initialized with a temperature of 0 K, the S_1-S_2 gap only reduces to ≈0.4 eV, leading to a transition probability of 10%. In the case of geometry optimization in the ID state where no kinetic energy is available, the gap reduces

TABLE 4: CC2/aug-cc-pVDZ Electronic Excitation Energies ω (eV), Stokes' Shifts Δ (eV), and Dipole Moments μ (Debye) of the S_1 Equilibrium Geometries Optimized at the CC2/TZVP Level[a]

CC2/aug-cc-pVDZ									
Conformer I				Conformer II				experimental	
ω	Δ		μ	ω	Δ		μ	ω	Δ
1.97	1.718	CT	17.7	2.12	1.562	CT	20.3	2.727(n-hexane[b]) 2.293(diethyl ether[c])	0.903 1.311
4.20		ID		4.15		ID			
4.33		CT		4.27		CT			
4.57		Rydberg		4.56		Rydberg			

[a] According to the single particle transitions, the excitations were labeled as charge transfer (CT), intra donor (ID) or Rydberg excitations. [b] The experimental fluorescence energy is taken from ref 13. [c] The experimental fluorescence energy is taken from ref 19.

Figure 6. Left: Newman projection along the N28−C9 bond of the CC2 structure optimized in S_2. Right: CC2 geometries optimized in S_0 (red) and optimized in S_1 (black), aligned on the donor unit.

TABLE 5: Calculated and Experimental[12] Values of the C9-Pyramidalization Angle (°) of Ground (S_0) and First Two Excited States (S_1 and S_2) Geometries of DA1[a]

	CC2	PBE	PBE0	X-ray
S_0	0.86	1.53	1.69	1.12
S_1	2.75(2.47)	−0.23	0.17	
S_2	−1.71			

[a] The C9-pyramidalization angle is defined as the average of the dihedrals N28−C10−C8−C9, C10−C8−N28−C9, and C8−N28−C10−C9. For CC2, the value of Conformer II (defined in Figure 4) is given in parentheses.

TABLE 6: CC2/aug-cc-pVDZ Excitation Energies ω (eV) and Dipole Moments μ (Debye) at the S_2 (ID) Equilibrium Geometry Optimized on CC2/TZVP Level

ω	assignment	μ
3.28	CT	19.7
3.83	ID	1.9
4.47	CT	5.4
4.68	Rydberg	6.5

only to about 0.6 eV (Table 6). These findings suggest that thermal energy is crucial to explain a fast interconversion.

After the transition to the CT state, the S_2-S_1 energy gap increases (Figure 7), making this reaction irreversible. If the system is kept artificially in the ID state (dashed lines in Figure 7), ID and CT states stay close to each other until the next AC is reached.

In the CT state the molecule adopts a strongly pyramidalized C3 center, and we observe a flipping between the two geometries that are similar to the two geometric minima of S_1 (see molecular snapshots in Figure 7). In the subsequent simulation time, the energy gap between S_1 and S_0 does not fall below 1.3 eV, indicating that a nonradiative decay channel is absent and the system can only relax to the ground state by emission of light.

To find the internal modes that decrease the energy gap we computed the gradient difference vector (GD) between S_1 and S_2 in the vicinity of an AC, i.e., after the system has overcome the initial activation barrier. The GD vector mainly leads to a

TABLE 7: Summary of the 8 Excited State AIMD Simulations[a]

P_{LZ}	$\Delta E(t_{min})$	t_{min}	E_A
96%	0.07	19	1.08
94%	0.09	13	0.63
94%	0.09	20	0.86
91%	0.27	20	1.17
91%	0.26	22	0.81
74%	0.23	19	0.66
64%	0.22	21	1.28
46%	0.20	28	0.34

[a] The Landau−Zener transition probabilities (P_{LZ}) are evaluated at the first avoided crossing (AC) after excitation into the ID state (S_2). t_{min} (fs) indicates the time at which the AC is reached, upon excitation. $\Delta E(t_{min})$ is the energy gap (eV) between S_2 and S_1 at the first AC. E_A (eV) is defined as the energy difference of S_2 at the AC ($t = t_{min}$) and at the Franck-Condon point ($t = 0$).

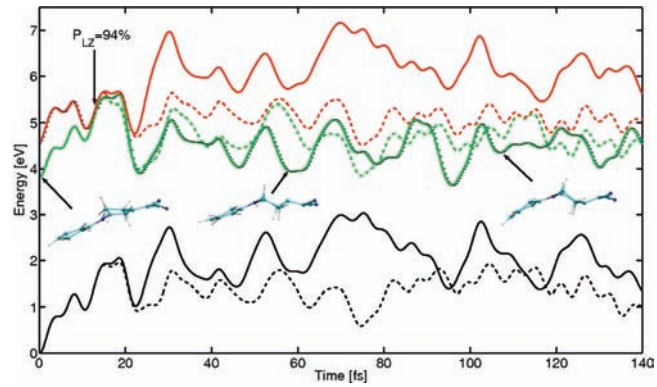

Figure 7. Potential energy as a function of time of a representative excited state MD simulation. Black, ground state; green, S_1; red, S_2. Solid curves correspond to the trajectory that jumps from S_2 to S_1 after 13 fs. The dashed line refers to a trajectory that was kept in S_2. The time where the surface hop occurs and the LZ probability (P_{LZ}) of the surface jump are indicated by the arrow.

distortion of the planarity of the phenyl substituent of the donor, and an increase of planarity at the C3 atom of the acceptor with simultaneous stretching of the C3−C12 bond. To further probe the PESs of the different electronic states with respect to this reaction coordinate, we displaced the atoms along the GD vector (Figure 8). Figure 8 shows that the minima of S_0 and ID state are very close to each other while the minimum of the CT state lies at larger GD displacements, corresponding to a larger C3-pyramidalization. In addition the intersection between CT and ID state is very close to the ID minimum but is higher in energy.

5. Conclusions

We have computed ground and excited state equilibrium structures, vertical excitation and fluorescence spectra by CC2

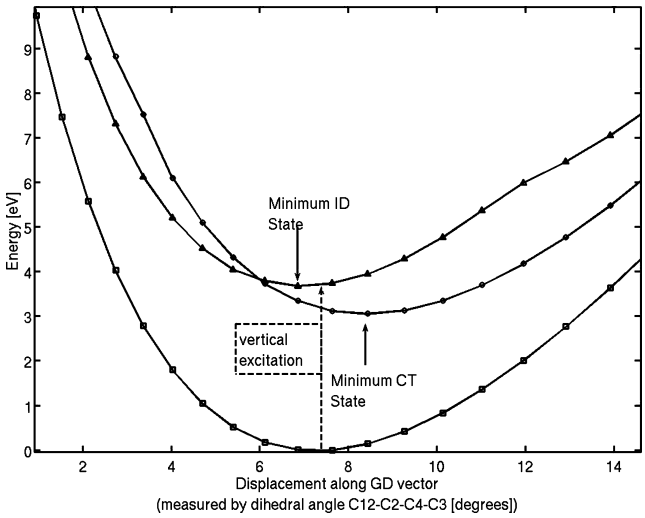

Figure 8. Potential energy curves for the ground state (squares), the ID state (triangles), and the CT state as a function of the C3 pyramidalization angle, measured by the C12−C2−C4−C3 dihedral angle. The geometries were obtained by displacing a geometry close to the AC along the GD vector.

and TDDFT methods. Furthermore, excited state ab initio (CC2) dynamics simulations have been carried out to simulate the internal conversion process from a locally excited state to a CT state.

Ground state geometries are well described by CC2 and the DFT methods we tested. A slightly smaller RMSD with respect to the crystal structure is found for DFT, especially using the PBE0 functional. However, all theoretical methods predict a twisted conformation of the phenyl group of the donor with respect to the central piperidine spacer, whereas the X-ray structure exhibits an almost symmetric conformation. Because of the fact that both, DFT and CC2 methods tend to yield more asymmetric conformations, we suspect that crystal packing effects are likely to be responsible for the more symmetric conformation of the phenyl group. A better answer to this question could be obtained by direct geometry optimization of the crystal using a method that accounts for weak interactions.[96]

The experimental vertical absorption energies are very well reproduced by CC2, enabling a full assignment of the experimental bands. Consistent with what suggested experimentally, we assign the lowest band at 3.63 eV to the fluorescent CT state. We assign the next higher absorption band at 4.25 eV to a $\pi-\pi^*$ ID excitation. According to CC2, the experimentally observed band at 4.9 eV is accounted for by two separate states, a CT and a Rydberg state.

In contrast to CC2, TDDFT underestimates the S_1 CT excitation by 1.4 eV using PBE and by 0.5 eV using PBE0. In addition, artificially low-lying CT states, which are not present in the CC2 spectra, are located between S_1 and the ID state in the case of PBE or mix considerably with the ID state in the case of PBE0. Although both TDDFT methods are able to reproduce the ID excitation energy within 0.4 eV, mixing of the artificial CT states with the locally excited ID state perturbs the potential energy surface of the ID state in such a way that neither geometry optimizations nor molecular dynamics calculations can be carried out in a pure ID state. This finding rules out the use of TDDFT to gain structural and dynamical information about the ID state. The common practice of using TDDFT to describe only the locally excited states by ignoring the presence of artificially too low lying CT states[97] cannot be applied for the present system due to the occurrence of strong mixing. In addition, excited state dipole moments are affected by the partial CT character.

The geometries of the zwitterionic structure of the first excited state appear to be different in the CC2 and the DFT description. Major characteristic of both, CC2 and TDDFT structures is an increase of the C3-pyramidalization on the acceptor, but geometries predicted by TDDFT exhibit a weaker pyramidalization at the N28 center than CC2. In addition, the N28 pyramidalization is slightly inverted compared to CC2.

Regarding fluorescence, CC2 is able to predict the emission energy within 0.2 eV compared to the value measured in diethyl ether, whereas a larger deviation of about 0.6 eV is found compared to the experimental value, measured in n-hexane. This could be due to a destabilization of the zwitterionic state by the solvent or by the approximations made in the CC2 model. To obtain more information about the effect of the solvent on the excitation energies a more sophisticated model[98] would be required.

Using CC2, we find a minimum energy structure for the ID state with a smaller S_2-S_1 energy gap than the S_0 geometry, but however still too large to allow for fast internal conversion from the ID (S_2) to the CT (S_2) state. In addition, we find the avoided crossing between ID and CT states to be higher in energy than the Franck−Condon region. Thus the interconversion requires thermal activation and can not be explained on the basis of single geometries only. Nonadiabatic excited state AIMD simulations reveal that at 300 K enough thermal energy is available to overcome the activation barrier and mediate a fast internal conversion. The process is triggered by a simultaneous stretching/pyramidalization of the ethylene acceptor moiety and a distortion of the planarity of the phenyl moiety of the donor. It occurs approximately 20 fs after preparation in the ID state.

Acknowledgment. We like to acknowledge useful discussions with Professor Filipp Furche. We thank the Swiss National Science Foundation (200020-116294) for financial support. E.T. acknowledges support of the Swiss National Science Foundation (PBELP2-125467) and the NSF Center on Chemistry at the Space-Time Limit at UCI (CHE-0533162).

Supporting Information Available: Additional tables of data. This material is available free of charge via the Internet at http://pubs.acs.org.

References and Notes

(1) Paddon-Row, M. N. Covalently Linked Systems Based on Organic Components. *Electron Transfer Chem.* **2001**, *3*, 179.
(2) Petty, M. C.; Bryce, M. R.; Bloor, In *An Introduction to Molecular Electronics*; Edward Arnold: London, 1995.
(3) Burroughes, J.; Bradley, D.; Brown, A.; Marks, R.; Mackay, K.; Friend, R.; Burns, P.; Holmes, A. *Nature* **1990**, *347*, 539–541.
(4) Joachim, C.; Gimzewski, J.; Aviram, A. *Nature* **2000**, *408*, 541–548.
(5) Hoffmann, R.; Imamura, A.; Hehre, W. J. *J. Am. Chem. Soc.* **1968**, *90*, 1499.
(6) Hoffmann, R. *Acc. Chem. Res.* **1971**, *4*, 1.
(7) Dougherty, D.; Hounshell, W.; Schlegel, H.; Bell, R.; Mislow, K. *Tetrahedron Lett.* **1976**, 3479–3482.
(8) Dougherty, D.; Schlegel, H.; Mislow, K. *Tetrahedron* **1978**, *34*, 1441–1447.
(9) Osawa, E.; Onuki, Y.; Mislow, K. *J. Am. Chem. Soc.* **1981**, *103*, 7475–7479.
(10) Osawa, E.; Ivanov, P.; Jaime, C. *J. Org. Chem.* **1983**, *48*, 3990–3993.
(11) Baldridge, K.; Battersby, T.; VernonClark, R.; Siegel, J. *J. Am. Chem. Soc.* **1997**, *119*, 7048–7054.
(12) Krijnen, B.; Beverloo, H. B.; Verhoeven, J. W.; Reiss, C. A.; Goubitz, K.; Heijdenrijk, D. *J. Am. Chem. Soc.* **1989**, *111*, 4433–4440.

(13) Hermant, R. M.; Bakker, N. A. C.; Scherer, T.; Krijnen, B.; Verhoeven, J. W. *J. Am. Chem. Soc.* **1990**, *112*, 1214.
(14) Pasman, P.; Verhoeven, J.; Deboer, T. *Chem. Phys. Lett.* **1978**, *59*, 381–391.
(15) vanDijk, S.; Groen, C.; Hartl, F.; Brouwer, A.; Verhoeven, J. *J. Am. Chem. Soc.* **1996**, *118*, 8425–8432.
(16) Aviram, A.; Ratner, M. *Chem. Phys. Lett.* **1974**, *29*, 277–283.
(17) Waldeck, D.; Beratan, D. *Science* **1993**, *261*, 576–577.
(18) Metzger, R. *J. Mater. Chem.* **1999**, *9*, 2027–2036.
(19) Schuddeboom, W.; Krijnen, B.; Verhoeven, J. W.; Staring, E. G. J.; Rikken, G. L. J. A.; Oevering, H. *Chem. Phys. Lett.* **1991**, *179*, 73.
(20) Bhanuprakash, K.; Rao, J. *Chem. Phys. Lett.* **1999**, *314*, 282–290.
(21) Sitha, S.; Rao, J.; Bhanuprakash, K.; Choudary, B. *J. Phys. Chem. A* **2001**, *105*, 8727–8733.
(22) Wegewijs, B.; Verhoeven, J. W. *Adv. Chem. Phys.* **1999**, *106*, 221–264.
(23) Lauteslager, X.; van Stokkum, I.; van Ramesdonk, H.; Bebelaar, D.; Fraanje, J.; Goubitz, K.; Schenk, H.; Brouwer, A.; Verhoeven, J. *Eur. J. Org. Chem.* **2001**, 3105–3118.
(24) Debreczeny, M.; Svec, W.; Marsh, E.; Wasielewski, M. *J. Am. Chem. Soc.* **1996**, *118*, 8174–8175.
(25) May, V.; Kühn, O. *Charge and Energy Transfer Dynamics in Molecular Systems*; Wiley-VCH: Weinheim, Germany, 2005.
(26) Pasman, P.; Verhoeven, J.; Deboer, T. *Tetrahedron Lett.* **1977**, 207–210.
(27) Pasman, P.; Rob, F.; Verhoeven, J. *J. Am. Chem. Soc.* **1982**, *104*, 5127–5133.
(28) Hoogesteger, F.; van Walree, C. A.; Jenneskens, L. W.; Roest, M. R.; Verhoeven, J. W.; Schuddeboom, W.; Piet, J. J.; Warman, J. M. *Chem.—Eur. J.* **2000**, *6*, 2948.
(29) Oosterbaan, W.; Koper, C.; Braam, T.; Hoogesteger, F.; Piet, J.; Jansen, B.; van Walree, C.; van Ramesdonk, H.; Goes, M.; Verhoeven, J.; Schuddeboom, W.; Warman, J.; Jenneskens, L. *J. Phys. Chem. A* **2003**, *107*, 3612–3624.
(30) Oosterbaan, W.; van Gerven, P.; van Walree, C.; Koeberg, M.; Piet, J.; Havenith, R.; Zwikker, J.; Jenneskens, L.; Gleiter, R. *Eur. J. Org. Chem.* **2003**, 3117–3130.
(31) Goes, M.; Verhoeven, J.; Hofstraat, H.; Brunner, K. *ChemPhysChem* **2003**, *4*, 349–358.
(32) Oosterbaan, W.; Kaats-Richters, V.; Jenneskens, L.; Walree, C. V. *J. Polym. Sci. Pol. Chem.* **2004**, *42*, 4775–4784.
(33) Moret, M.; Tapavicza, E.; Guidoni, L.; Röhrig, U. F.; Sulpizi, M.; Tavernelli, I.; Rothlisberger, U. *Chimia* **2005**, *59*, 493–498.
(34) Barolo, C.; Nazeeruddin, M.; Fantacci, S.; Censo, D. D.; Comte, P.; Liska, P.; Viscardi, G.; Quagliotto, P.; Angelis, F. D.; Ito, S.; Graetzel, M. *Inorg. Chem.* **2006**, *45*, 4642–4653.
(35) Ghosh, S.; Chaitanya, G.; Bhanuprakash, K.; Nazeeruddin, M.; Graetzel, M.; Reddy, P. *Inorg. Chem.* **2006**, *45*, 7600–7611.
(36) Belletete, M.; Blouin, N.; Boudreault, P.; Leclerc, M.; Durocher, G. *J. Phys. Chem. A* **2006**, *110*, 13696–13704.
(37) Nazeeruddin, M.; Bessho, T.; Cevey, L.; Ito, S.; Klein, C.; Angelis, F. D.; Fantacci, S.; Comte, P.; Liska, P.; Imai, H.; Graetzel, M. *J. Photochem. Photobiol. A-Chem.* **2007**, *185*, 331–337.
(38) Mete, E.; Uner, D.; Cakmak, M.; Gulseren, O.; Ellialtoglu, S. *J. Phys. Chem. C* **2007**, *111*, 7539–7547.
(39) Angelis, F. D.; Fantacci, S.; Sgamellotti, A. *Theor. Chem. Acc.* **2007**, *117*, 1093–1104.
(40) Hagberg, D.; Marinado, T.; Karlsson, K.; Nonomura, K.; Qin, P.; Boschloo, G.; Brinck, T.; Hagfeldt, A.; Sun, L. *J. Org. Chem.* **2007**, *72*, 9550–9556.
(41) Belletete, M.; Boudreault, P.; Leclerc, M.; Durocher, G. *Theochem.-J. Mol. Struct.* **2007**, *824*, 15–22.
(42) Tsai, M.; Hsu, Y.; Lin, J.; Chen, H.; Hsu, C. *J. Phys. Chem. C* **2007**, *111*, 18785–18793.
(43) Christiansen, O. *Theor. Chem. Acc.* **2006**, *116*, 106–123.
(44) Christiansen, O.; Koch, H.; Jørgensen, P. *Chem. Phys. Lett.* **1995**, *243*, 409–418.
(45) Köhn, A.; Hättig, C. *J. Chem. Phys.* **2003**, *119*, 5021–5036.
(46) Hättig, C. *J. Chem. Phys.* **2003**, *118*, 7751–7761.
(47) Christiansen, O.; Koch, H.; Jørgensen, P.; Helgaker, T. *Chem. Phys. Lett.* **1996**, *263*, 530–539.
(48) Christiansen, O.; Koch, H.; Halkier, A.; Jørgensen, P.; Helgaker, T.; de Meras, A. *J. Chem. Phys.* **1996**, *105*, 6921–6939.
(49) Fliegl, H.; Köhn, A.; Hättig, C.; Ahlrichs, R. *J. Am. Chem. Soc.* **2003**, *125*, 9821–9827.
(50) Sobolewski, A. L.; Domcke, W.; Hättig, C. *J. Phys. Chem. A* **2006**, *110*, 6301–6306.
(51) Hättig, C.; Hellweg, A.; Köhn, A. *J. Am. Chem. Soc.* **2006**, *128*, 15672–15682.
(52) Sobolewski, A. L.; Domcke, W. *Phys. Chem. Chem. Phys.* **2006**, *8*, 3410–3417.
(53) Perun, S.; Sobolewski, A. L.; Domcke, W. *J. Phys. Chem. A* **2006**, *110*, 13238–13244.
(54) Fabiano, E.; Sala, F. D.; Barbarella, G.; Lattante, S.; Anni, M.; Sotgiu, G.; Hättig, C.; Cingolani, R.; Gigli, G.; Piacenza, M. *J. Phys. Chem. B* **2007**, *111*, 490–490.
(55) Fleig, T.; Knecht, S.; Hättig, C. *J. Phys. Chem. A* **2007**, *111*, 5482–5491.
(56) Hellweg, A.; Hättig, C. *J. Chem. Phys.* **2007**, *127*, 024307.
(57) Sobolewski, A. L.; Domcke, W. *Phys. Chem. Chem. Phys.* **2007**, *9*, 3818–3829.
(58) Sobolewski, A. L.; Domcke, W. *Chem. Phys. Lett.* **2008**, *457*, 404–407.
(59) Sobolewski, A. L.; Domcke, W. *J. Phys. Chem. A* **2008**, *112*, 7311–7313.
(60) Runge, E.; Gross, E. *Phys. Rev. Lett.* **1984**, *52*, 997–1000.
(61) Casida, M. E. Time-dependent density-functional response theory for molecules. *Recent Adv. Density Funct. Methods* **1995**, 155.
(62) Marques, M.; Gross, E. *Lect. Notes. Phys.* **2003**, *620*, 144–184.
(63) Sobolewski, A. L.; Domcke, W. *Eur. Phys. J. D* **2002**, *20*, 369–374.
(64) Marques, M.; Lopez, X.; Varsano, D.; Castro, A.; Rubio, A. Phys. Rev. Lett. 2003, *90*.
(65) Sobolewski, A. L.; Domcke, W. *J. Phys. Chem. A* **2004**, *108*, 10917–10922.
(66) Rappoport, D.; Furche, F. *J. Am. Chem. Soc.* **2004**, *126*, 1277–1284.
(67) Dreuw, A. *ChemPhysChem* **2006**, *7*, 2259–2274.
(68) Cordova, F.; Doriol, L. J.; Ipatov, A.; Casida, M. E.; Filippi, C.; Vela, A. *J. Chem. Phys.* **2007**, *127*, 164111.
(69) Tapavicza, E.; Tavernelli, I.; Rothlisberger, U. *Phys. Rev. Lett.* **2007**, *98*, 023001.
(70) Tapavicza, E.; Tavernelli, I.; Rothlisberger, U.; Filippi, C.; Casida, M. E. *J. Chem. Phys.* **2008**, *129*, 124108.
(71) Tavernelli, I.; Tapavicza, E.; Rothlisberger, U. *J. Chem. Phys.* **2009**, *130*, 124107.
(72) Tavernelli, I.; Tapavicza, E.; Rothlisberger, U. *J. Mol. Struct.* 2009, in press, doi: 10.1016/j.theochem.2009.04.020.
(73) Maitra, N.; Tempel, D. *J. Chem. Phys.* **2006**, *125*, 184111.
(74) Dreuw, A.; Weisman, J.; Head-Gordon, M. *J. Chem. Phys.* **2003**, *119*, 2943–2946.
(75) Ploetner, J.; Dreuw, A. *Chem. Phys.* **2008**, *347*, 472–482.
(76) Parusel, A.; Köhler, G.; Grimme, S. *J. Phys. Chem. A* **1998**, *102*, 6297–6306.
(77) Jamorski, C.; Foresman, J.; Thilgen, C.; Lüthi, H. *J. Chem. Phys.* **2002**, *116*, 8761–8771.
(78) Jamorski Jödicke, C.; Lüthi, H. *J. Am. Chem. Soc.* **2003**, *125*, 252–264.
(79) Ahlrichs, R.; Bär, M.; Häser, M.; Horn, H.; Kölmel, C. *Chem. Phys. Lett.* **1989**, *162*, 165–169.
(80) Weigend, F.; Häser, M.; Patzelt, H.; Ahlrichs, R. *Chem. Phys. Lett.* **1998**, *294*, 143.
(81) Woon, D. E.; Dunning, T. H. *J. Chem. Phys.* **1993**, *98*, 1358–1371.
(82) Hirata, S.; Head-Gordon, M. *Chem. Phys. Lett.* **1999**, *314*, 291–299.
(83) Hättig, C.; Weigend, F. *J. Chem. Phys.* **2000**, *113*, 5154–5161.
(84) Hättig, C.; Köhn, A. *J. Chem. Phys.* **2002**, *117*, 6939–6951.
(85) Weigend, F.; Häser, M. *Theor. Chem. Acc.* **1997**, *97*, 331–340.
(86) Weigend, F.; Köhn, A.; Hättig, C. *J. Chem. Phys.* **2002**, *116*, 3175–3183.
(87) Häser, M.; Ahlrichs, R. *J. Comput. Chem.* **1989**, *10*, 104.
(88) Bauernschmitt, R.; Ahlrichs, R. *Chem. Phys. Lett.* **1996**, *256*, 454.
(89) Furche, F.; Ahlrichs, R. *J. Chem. Phys.* **2002**, *117*, 7433–7447.
(90) Bauernschmitt, R.; Ahlrichs, R. *J. Chem. Phys.* **1996**, *104*, 9047.
(91) Perdew, J.; Burke, K.; Ernzerhof, M. *Phys. Rev. Lett.* **1996**, *77*, 3865–3868.
(92) Jarikov, V.; Neckers, D. *J. Org. Chem.* **2001**, *66*, 659–671.
(93) Lauteslager, X.; Wegewijs, B.; Verhoeven, J.; Brouwer, A. *J. Photochem. Photobiol. A-Chem.* **1996**, *98*, 121–126.
(94) Lauteslager, X.; Bartels, M.; Piet, J.; Warman, J.; Verhoeven, J.; Brouwer, A. *Eur. J. Org. Chem.* **1998**, 2467–2481.
(95) Jones, G. A.; Carpenter, B. K.; Paddon-Row, M. N. *J. Am. Chem. Soc.* **1990**, *120*, 5499–5508.
(96) Tapavicza, E.; Lin, I.-C.; von Lilienfeld, O. A.; Tavernelli, I.; Coutinho-Neto, M. D.; Rothlisberger, U. *J. Chem. Theory Comput.* **2007**, *3*, 1673–1679.
(97) Mercier, S. R.; Boyarkin, O. V.; Kamariotis, A.; Guglielmi, M.; Tavernelli, I.; Cascella, M.; Rothlisberger, U.; Rizzo, T. R. *J. Am. Chem. Soc.* **2006**, *128*, 16938–16943.
(98) Nemykin, V.; Hadt, R.; Belosludov, R.; Mizuseki, H.; Kawazoe, Y. *J. Phys. Chem. A* **2007**, *111*, 12901–12913.

JP901356K